Remote Sensing of Environment 178 (2016) 104–112

Contents lists available at ScienceDirect

Remote Sensing of Environment

journal homepage: www.elsevier.com/locate/rse

Dominant backscattering mechanisms at L-band during dynamic soil moisture conditions for sandy soils

Pang-Wei Liu [a,*], Jasmeet Judge [a], Roger D. DeRoo [b], Anthony W. England [c,d], Tara Bongiovanni [a], Adam Luke [e]

[a] Center for Remote Sensing, Agricultural and Biological Engineering Department, Institute of Food and Agricultural Sciences, University of Florida, Gainesville, USA
[b] Department of Climate and Space Sciences and Engineering, University of Michigan-Ann Arbor, Ann Arbor, MI, USA
[c] Department of Electrical Engineering and Computer science, University of Michigan-Ann Arbor, Ann Arbor, MI, USA
[d] College of Engineering and Computer Science, University of Michigan-Dearborn, Dearborn, MI, USA
[e] Department of Civil and Environmental Engineering, University of California-Irvine, Irvine, CA, USA

ARTICLE INFO

Article history:
Received 28 July 2015
Received in revised form 18 February 2016
Accepted 27 February 2016
Available online 14 March 2016

Keywords:
Active microwave remote sensing
Radar
NASA-NISAR
JAXA-ALOS2
Soil moisture
Surface scattering
Volume scattering

ABSTRACT

In this study, we investigate dominant backscattering mechanisms under different soil moisture (SM) and roughness conditions for bare sandy soils, and discuss potential impacts on active microwave algorithms for soil moisture estimation. This study used ground-based observations of backscattering coefficient (σ^0) over three drydown periods. Under rough soil conditions, surface scattering was the dominant mechanism during both dry and wet periods, and the σ^0 followed a power-law relationship with SM, with R^2 values > 0.86. However, under smooth soil conditions, the relationship was negative for SM < 0.07 m^3/m^3. A simple volume scattering model was used to provide plausible explanation for such a behavior due to volume scattering. Sensitivities of σ^0 to SM using both observed and modeled σ^0 were analyzed. The observed sensitivity was higher for smooth soil than that for rough soil, when surface scattering was the dominant mechanism, while the sensitivity estimated by the AIEM model was largely unaffected by surface roughness. Observations at VV-pol were more sensitive to SM than at other polarizations by up to 1 dB/0.01m^3/m^3 for rough soil, while the AIEM model estimated similar sensitivities at both VV and HH-pol, with the maximum difference between the modeled and observed sensitivities of 3 dB/0.01m^3/m^3. This study demonstrates that volume scattering under dry, smooth conditions and a non-linear relationship between σ^0 and SM under rough conditions in sandy soils may have significant impacts on estimate of SM using active algorithms.

1. Introduction

Soil moisture (SM) is one of the critical factors for predicting moisture fluxes such as evapotranspiration, surface runoff, infiltration, and recharge, as well as crop growth and yield (Judge, 2007). Remotely sensed observations at microwave frequencies are sensitive to changes in water content for the top few centimeters of soil. Observations at L-band (1–2 GHz) are preferred due to their minimal extinction in the atmosphere and better penetration through vegetation. Satellite-based radar systems allow frequent observations for SM studies with global coverage. For example, the Japan Aerospace Exploration Agency (JAXA) Advanced Land Observing Satellite-2 (ALOS-2) provides fully polarimetric (full-pol) observations at a frequency of 1.26 GHz at a spatial resolution of 6.5–100 m, with a repeat coverage of 14 days (Balenzano et al., 2013; Suzuki, Osawa, Hatooka, Kankaku, & Watanabe, 2009). The National Aeronautics and Space Administration (NASA) and Indian Space Research Organization (ISRO) SAR (NISAR) mission (Rosen et al., 2015), scheduled for launch in 2020, will provide full-pol observations every 12 days at a frequency of 1.26 GHz, with a spatial resolution of 10 m.

Compared to the passive techniques, less progress has been made in utilizing active microwave signatures for SM (Barrett, Dwyer, & Whelan, 2009), primarily because they are highly sensitive to the surface roughness and vegetation structure in addition to SM. In the past decades, efforts have been made to understand the relationship between L-band backscattering coefficient (σ^0) to the SM and backscattering mechanisms using either airborne (Kim & van Zyl, 2009; Narayan, Lakshmi, & Jackson, 2006; Oh, Sarabandi, & Ulaby, 2002), or ground-based observations (Dobson & Ulaby, 1986; Oh, Sarabandi, & Ulaby, 1992) for development of active algorithms. These studies were conducted for VSM > 10% and have found different relationships between σ^0 and SM, and hence sensitivity, due to variations in surface roughness, vegetation, and soil textures. Findings from these studies may not be applicable to sandy soils, one of the predominant soil types in Florida, USA, because of their high drainage rates. In addition, because the radar at L-band is capable of penetrating through the soil surface (Paillou et al., 2003; Schaber, McCauley, Breed, & Olhoeft, 1986), the volume scattering, that could complicate the modeling of σ^0 for SM, may be considered, particularly for co-pol observations of σ^0 in smooth, dry soils (Shi, van

* Corresponding author.
E-mail address: bonwei@ufl.edu (P.-W. Liu).

http://dx.doi.org/10.1016/j.rse.2016.02.062
0034-4257/

Zyl, Soares, & Engman, 1992; Ulaby, Moore, & Fung, 1982). Theoretical analyses and derivations have been used to understand surface and volume scattering mechanisms (Fung, 1994; Nashashibi, Ulaby, & Sarabandi, 1996; Onier et al., 2011). These studies attributed the differences between the observed and modeled σ^0 to the impacts of volume scattering. However, a gap still remains in identifying the *transition* of dominant scattering mechanisms at lower frequencies, such as at L-band, primarily due to lack of frequent observations of the dry soil to capture its dynamics. Current ground-based systems (Kim, Jackson, Bindlish, Lee, & Hong, 2012; Kurum et al., 2011; Nagarajan et al., 2014) offer unprecedented capabilities to obtain frequent, long-term observations during dynamic conditions. Such studies can provide insights into the conditions of applicability for the current SM retrieval algorithms (Das, Entekhabi, & Njoku, 2011).

The University of Florida L-band Automated Radar System (UF-LARS) provides continuous quad-polarized measurements every 15 min, day and night, and even during hydrologic events such as precipitation and irrigation. Thus, the UF-LARS observations are applicable for identification of scattering mechanisms over a wide range of SM values. The goal of this study is to understand dominant backscattering mechanisms and their transitions, and the sensitivity of σ^0 to SM under dynamic conditions for sandy agricultural soils using high temporal density observations from UF-LARS. The objectives of this study are to 1) investigate observed backscattering mechanisms and relationship between σ^0 and SM for smooth and rough sandy soils under different moisture conditions, 2) provide a plausible explanation for the observed behavior using a physically-based scattering model, and 3) evaluate the sensitivity of the observed and modeled σ^0 to SM. Findings of this study provide insights into development of active algorithms for SM estimates and data assimilation for sandy soils.

2. Experimental observations

2.1. MicroWEX-11

The Microwave, Water, and Energy Balance Experiments (MicroWEXs) are a series of season-long experiments conducted at the Plant Science Research and Education Unit (PSREU), Institute of Food and Agricultural Sciences (IFAS), in north central Florida, to monitor the microwave signatures of soil and vegetation during different stages of growth. Soil texture at the field site is sandy, consisting of 89.4% by vol. of sand, 7.1% by vol. of clay, and 3.5% by vol. of silt. A bare soil experiment was conducted in 2012 during the eleventh MicroWEX (MicroWEX-11) from May 9 (Day of year (DoY) 130) to June 8 (DoY 160). Concurrent observations of active and passive observations were conducted at L-band. In this paper, we report observations of microwave backscatter from soil in an unvegetated agricultural field using UF-LARS. The UF-LARS operated at the frequency of 1.25 GHz ($\lambda = 24.0$ cm), and observed backscatter at four polarization combinations, VV, HH, HV, and VH every 15 min. Measurements were conducted at a height of 16.2 m above the ground with an incidence angle of 40°. Details of electro-mechanical and control systems in UF-LARS are published in Nagarajan et al. (2014).

Five SM profiles were observed near the UF-LARS footprint using Campbell Scientific CS616 Time Domain Reflectometry (TDR) sensors at depths of 2, 4, 8, 16, 32, and 64 cm, as shown in Fig. 1. A site specific calibration for sandy soils was applied to obtain VWC from the sensor measurements, and the calibration error of a TDR sensor was found to be 0.011 m^3/m^3. For this study, observations at 2 cm from these five profiles were averaged to represent near-surface SM in the radar footprint. The averaged standard deviation of SM observations at 2 cm from five profiles over the period of the experiment is 0.010 m^3/m^3 indicating that the variability between the five locations was very small, so the soil in the footprint is considered homogeneous. As a result, the total averaged uncertainty in the VSM observations was ~0.012 m^3/m^3 based upon the Student's *t*-test with a confidence interval of 95%.

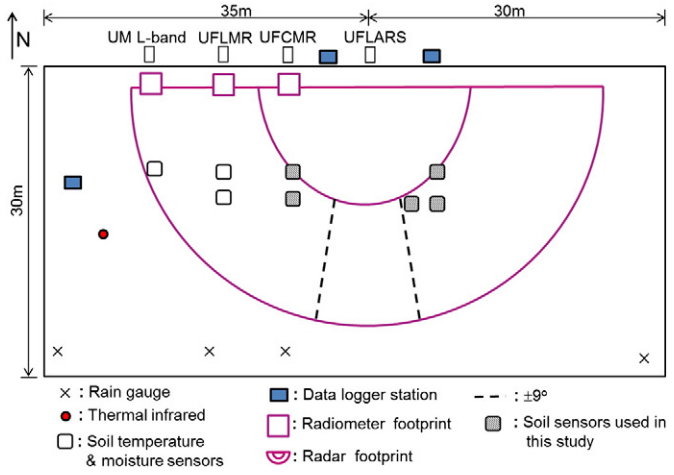

Fig. 1. Sensor layout in the field for the bare soil experiment during MicroWEX-11. Row structure was in the east-west direction during rough periods, and 0° azimuth for radar observation is due south. Dashed lines represent the limits of the observation between ±9° used in this study.

Four rain gauges were used to record the amount of water input during the irrigation/precipitation events. A linear move irrigation system was used to maintain uniform water application to the field. In the beginning of the experiment on DoY 122, the field was disced to achieve a smooth soil surface, as typically prepared prior to planting. Observations for smooth soils were used 8 days later, on DoY 130, when the soil had settled down and was naturally smoothed. After 23 days, on DoY 145, a seedless planting was conducted in east–west direction (see Fig. 1), providing a typical soil roughness during the planting and germination stages. Soil roughness measurements, including root mean square height (s) and correlation length (l), were conducted across and along the rows during the smooth period on DoY 132 and 138, and during the rough period on DoY 146 and 163. This study used observations from six 2D surface profiles, in the direction perpendicular and parallel to the row structure of the field with a 2 m-long mesh board for each roughness measurement. The surface profile from each mesh board was digitized to calculate s and l (Yang, Tien, Casanova, & Judge, 2005), individually. Each soil roughness measurement was acquired by averaging six s and l values, listed in Table 1. Because the surface roughness may be underestimated using a 2-m soil profile (Baghdadi, Paillou, Grandjean, & Davidson, 2000), the roughness measurements were modified using a correction equation, given as (Nishimoto, 2010):

$$\hat{l} = l + \frac{l^2(e-1)\sqrt{\pi}}{L} \tag{1a}$$

$$\hat{s} = \left[1 - \frac{2\hat{l}\sqrt{\pi}}{L}\right]^{-1} s^2 \tag{1b}$$

where, L is the length of soil profile in cm, and $\hat{s}$ and $\hat{l}$ are corrected root mean square height and correlation length in cm, respectively, listed in Table 1.

Table 1
Soil surface roughness measurements of root mean square height (s) and correlation length (l) using 2 m-long mesh board during MicroWEX-11, and their corrected values using (Nishimoto, 2010).

DoY (2012)	Perpendicular				Parallel			
	s (cm)	l (cm)	$\hat{s}$ (cm)	$\hat{l}$ (cm)	s (cm)	l (cm)	$\hat{s}$ (cm)	$\hat{l}$ (cm)
132	0.68	9.80	0.80	11.26	0.32	6.76	0.34	7.46
138	0.70	9.33	0.82	10.66	0.35	11.60	0.40	13.65
146	1.71	9.45	1.90	10.81	0.45	1.78	0.46	1.83
163	1.30	12.22	1.51	14.47	0.32	10.68	0.36	12.42

Table 2
The specifications of the UF-LARS.

Parameter	Qualifier	UF-LARS
Frequency (GHz)	Center	1.25
Bandwidth (GHz)		0.3
Beamwidth (deg)	3 dB	14.7 & 19.7 in E- & H-Planes
Polarization isolation (dB)	Center/edge	>37/23
Polarization		HH, VV, VH, and VH
NEσ^0 (dB)	HH/VV/VH/HV	−23.42/−25.58/−48.12/−38.84

2.2. UF-LARS data processing and calibration

The UF-LARS is a Network Analyzer (NWA) based system to provide magnitude and phase of the power ratio measurements at the four polarization combinations from 1100–1400 MHz with a 1.5 MHz increment. Table 2 lists specifications of the UF-LARS. Signal processing and calibration procedure, consisting of internal calibration, time gating processing, and external calibration using a trihedral corner-reflector were conducted to obtain σ^0 from the received signal as described in (Nagarajan et al., 2014).

Averaging independent samples in space and/or frequency to obtain a mean amplitude of radar return is necessary to reduce the uncertainty of a radar measurement caused by fading. Observations of σ^0 were averaged over measurements obtained spatially along three azimuthal scans at −9°, 0°, and +9° with respect to due South (see Fig. 1), and nine frequency measurements at 30 MHz increments from 1130–1370 MHz at each azimuth angle. The agricultural row effect to σ^0 variation was minimal within these angles (Ulaby, Kouyate, Fung, & Sieber, 1982). The frequency measurements met the spectral independence criterion of $\Delta f \geq \frac{c}{2\Delta r}$, where Δf is the difference between two adjacent frequencies, c is the speed of light, and the Δr is the difference between the maximum and minimum ranges from the antenna to the effective illuminated area of the target (Ulaby & Dobson, 1989). In all, 27 samples were averaged for a backscattering measurement and the standard deviation of fading was decreased from 5.57 to 0.85 dB (Hoekman, 1991). The

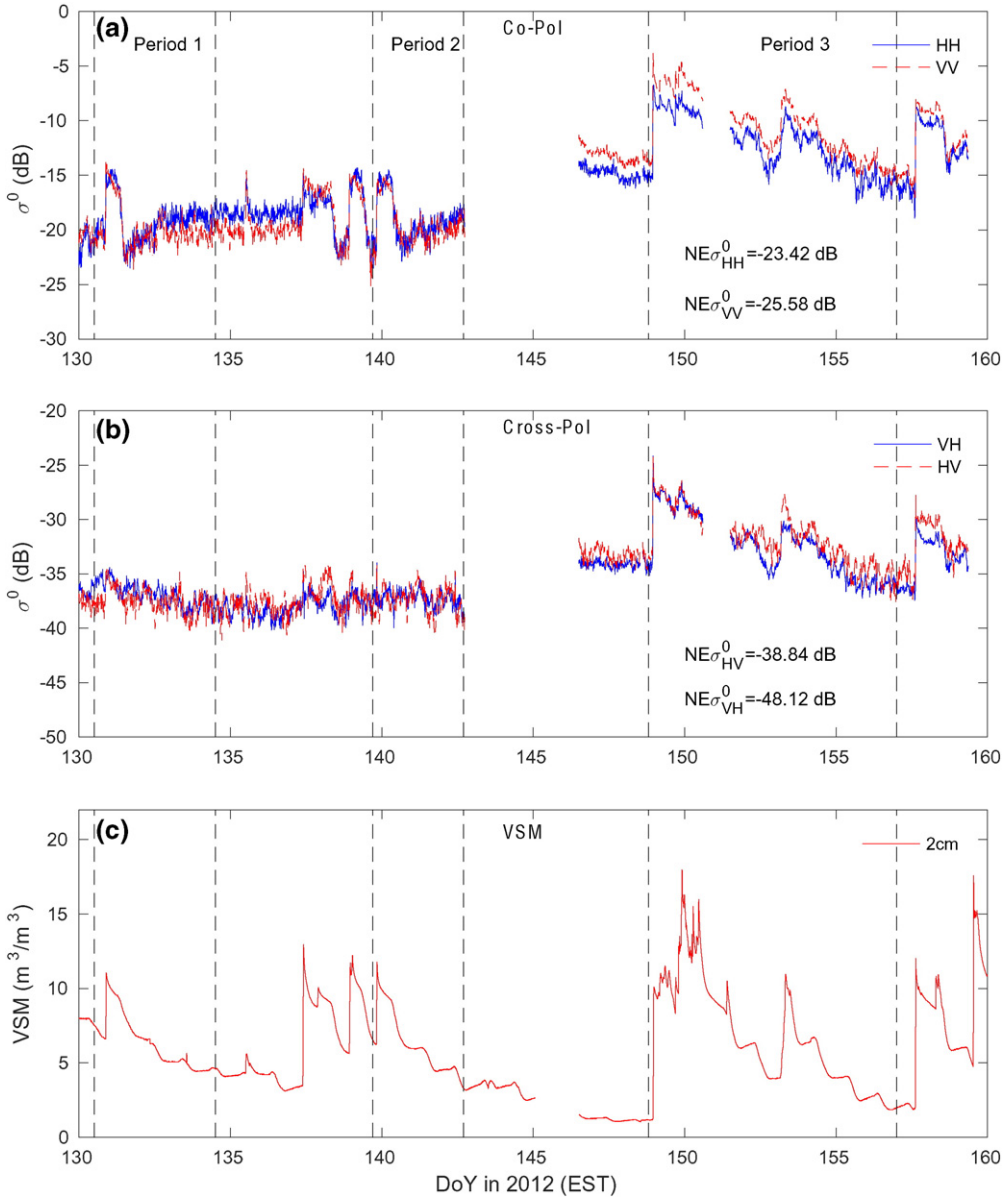

Fig. 2. Plots show σ^0_{HH}, σ^0_{VV}, σ^0_{VH}, and σ^0_{HV} and the VSM at 2 cm, which were observed concurrently during the bare soil experiment. (a) σ^0 at Co-pol, (b) σ^0 at Cross-pol, and (c) VSM. The drydown of periods 1 and 2 were under smooth condition while period 3 was under rough condition of sandy soil. They are described in detail in Section 4.1.

errors from various calibration sources were obtained from (Nagarajan et al., 2014), and the overall uncertainty of radar measurements can be quantified to be 1.71 dB.

Fig. 2 shows the observed σ^0 at the four polarization combinations at an incidence angle of 40° and VSM observed at 2 cm during the bare soil experiment. The theoretical amplitudes of backscatter from same target at VH- and HV-pol are identical, i.e. $\sigma^0_{VH} = \sigma^0_{HV}$. After removing the post-calibration residual bias between the two signal paths, the RMSD between σ^0_{VH} and σ^0_{HV} was found to be 0.99 dB. This value is similar to the random noise of 0.85 dB due to fading. In this study, σ^0_{VH} were used as the cross-pol measurements, σ^0_{cr}.

3. Scattering models

3.1. Surface scattering model

In this study, the physically-based, Advanced Integral Equation Model (AIEM), was used to compute the surface backscattering of soil (σ^0_{soil}), given as (Chen et al., 2003):

$$\sigma^0_{soil,pq}(\theta_i,\phi_i;\theta_s,\phi_s) = \frac{k^2}{2}\exp\left[-s^2\left(k_z^2+k_{sz}^2\right)\right]\cdot\sum_{n=1}^{\infty}\frac{s^{2n}}{n!}\left|I^n_{pq}\right|^2 W^{(n)}(k_{sx}-k_x,k_{sy}-k_y) \tag{2a}$$

$$\begin{aligned} k_x &= k\sin\theta_i\cos\phi_i \quad ; \quad k_{sx} = k\sin\theta_s\cos\phi_s \\ k_y &= k\sin\theta_i\sin\phi_i \quad ; \quad k_{sy} = k\sin\theta_s\sin\phi_s \\ k_z &= k\cos\theta_i \quad ; \quad k_{sz} = k\cos\theta_s \end{aligned} \tag{2b}$$

where k is the wavenumber in the air ($\frac{2\pi}{\lambda}$), s is the rms height of the terrain surface, (θ_i, ϕ_i) and (θ_s, ϕ_s) are elevation and azimuth angles for the incident and the scattered radiation, respectively, I^n_{pq} is a function consisting of Kirchhoff and complementary field coefficients defined in (Chen et al., 2003), and $W^{(n)}$ is the Fourier transform of the n^{th} power of the normalized surface correlation function. In this study, the transition model was used for Fresnel reflection coefficient (Wu, Chen, Shi, Lee, & Fung, 2008) and the exponential correlation function was used for the $W^{(n)}$ because it is more representative of the natural terrain than the Gaussian function (Fung & Kuo, 2006; Oh et al., 1992). Validity ranges of normalized root mean square height (ks) and correlation length (kl) for the AIEM are 0.20–2.58 and 1.07–8.36, respectively (Chen et al., 2003), and the surface roughness conditions in the field were within these ranges. The dielectric constant of soil (ϵ_{soil}) was obtained from a mineralogically-based model (Mironov, Kosolapova, & Fomin, 2009). Fig. 3 shows the relationship between the real and imaginary parts of ϵ_{soil} to VSM for sandy soils. The real part increases from 3 to 12 as the moisture increases from 0.02 to 0.2 m^3/m^3.

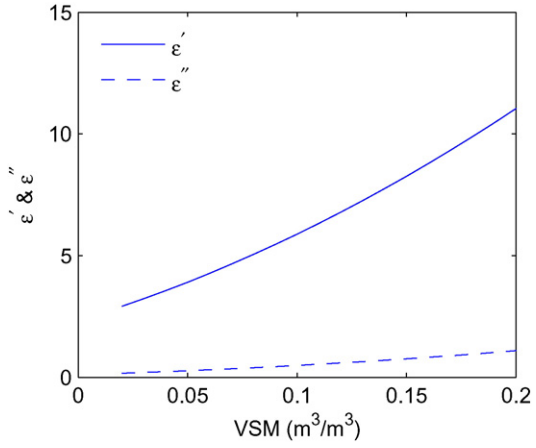

Fig. 3. Real and imaginary parts of ϵ_{soil}, ϵ' and ϵ'', to VSM using mineralogically-based model (Mironov et al., 2009), with sand and clay fractions of 89.4% and 3.5% by volume, respectively.

3.2. Volume scattering model

To provide a plausible explanation for the negative slope observed in the co-pol backscattering due to volume scattering, a zero-order approximation model for volume scattering ($\sigma^0_{pp,vol}$) was used in this study, given as (Fung, 1994):

$$\sigma^0_{pp,vol} = (1-\Gamma_p)^2\int_0^{\delta_p}\sigma_s(z)N_s(z)e^{(-2\kappa_e z\ \sec\theta_i)}dz \tag{3}$$

where, p is the polarization, Γ is the Fresnel reflectivity, and δ_p is the theoretical penetration depth of soil, given as (Ulaby, Moore, et al., 1982):

$$\delta_p = \frac{1}{2k\left|Im\left[\sqrt{\epsilon_{soil}}\right]\right|} \tag{4}$$

The soil medium consisted of moist soil particles and air, where σ_s represents radar cross sections (RCS) of a soil particle, N_s represents numbers of soil particles per unit area, and κ_e is the extinction coefficient of the soil medium. In this study, the σ_s was estimated using the Rayleigh approximation as its particle size was small compared to the wavelength of L-band (Ulaby, Moore, & Fung, 1981).

Using the Rayleigh approximation, the RCS of a soil particle is the function of its dielectric constant (ϵ_s) and radius (r_s), and wavelength of radar signal (λ), given as (Ulaby et al., 1981):

$$\sigma_s = 4\pi r_s^2\chi^4|K|^2 \tag{5a}$$

$$\chi = \frac{2\pi r_s}{\lambda}\sqrt{Re\left[\epsilon_{bg}\right]} \tag{5b}$$

$$K = \frac{n^2-1}{n^2+2} \tag{5c}$$

where, the ϵ_{bg} is the dielectric constant of the background, which is air in this study (ie. $\epsilon_{bg} = 1$), the λ of UF-LARS is 24 cm, and n is the ratio of refraction indices of the soil particle and background as $\sqrt{\frac{\epsilon_s}{\epsilon_{bg}}}$.

Sandy soils range from fine sand to cluster (or clod) with particle radii from 0.03 to 15 mm (Onier et al., 2011; USDA, 1987). In this study, we used a soil particle radius (r_s) of 3 mm, within the range, given our field conditions of sandy soil with small clusters. The dielectric constant of the soil particle (ϵ_s) was modeled by consisting of solid soil (ϵ_{ss}), bound water (ϵ_{bw}), and free water (ϵ_{fw}) given as:

$$\epsilon_s = \left(\epsilon_{ss}^{1/2}\frac{f_{ss}}{f_{ss}+VSM} + \epsilon_{bw}^{1/2}\frac{f_{bw}}{f_{ss}+VSM} + \epsilon_{fw}^{1/2}\frac{VSM-f_{bw}}{f_{ss}+VSM}\right)^2 \tag{6}$$

where, ϵ_{ss} and ϵ_{bw} were estimated by using mineralogically-based equations (Mironov et al., 2009), and ϵ_{fw} was estimated from Debye relaxation (Ulaby, Moore, & Fung, 1986). The f_{ss} is the fraction of solid soil defined as $\frac{\rho_b}{\rho_s}$, in which $\rho_b = 1.51$ g/cm^3 is the bulk density and $\rho_s = 2.40$ g/cm^3 is the specific density of soil particle, measured from a soil texture analysis (Bongiovanni et al., 2015). The f_{bw} is the fraction of bound water in the soil medium, which is the same as VSM when the VSM < maximum bound water (W_{vt}) of soil, but equals to W_{vt} when VSM ≥ W_{vt}. The W_{vt} was set at 0.02 m^3/m^3 for sandy soil (Mironov & Bobrov, 2009). The free water occurs when VSM > W_{vt}; otherwise the last term in Eq. (6) is neglected.

N_s was obtained from Eq. (7) with the soil particle uniformly distributed in the soil medium (Fung, 1994).

$$N_s = \frac{3f_{ss}}{4\pi r_s^3} \tag{7}$$

The κ_e includes the scattering coefficient of particles (κ_s) and the absorption coefficient of moist soil medium (κ_a) defined as (Fung, 1994; Ulaby et al., 1986):

$$\kappa_s = \frac{8}{3} N_s \pi r^2 \chi^4 |K|^2 \tag{8a}$$

$$\kappa_a = 2k\,Im[\sqrt{\epsilon_{soil}}]. \tag{8b}$$

4. Methodology

4.1. Scattering mechanisms

In this study, three drydown periods were selected to investigate backscattering mechanisms of bare soil under different moisture and roughness conditions. Two periods were during the smooth period from DoY 130.5 to 134.5 and DoY 139.7 to 142.7, and one was during the rough period from DoY 148.8 to 157, after the seedless planting was conducted, as shown in Fig. 2. Table 3 provides information regarding water input and the moisture range during these drydown periods. Due to the high drainage rate of sandy soils, the observed SM was $<0.20\ m^3/m^3$ during the entire experiment. A total of 380, 285, and 690 radar observations were conducted during drydown periods 1, 2, and 3, respectively, providing detailed information regarding change of VSM, particularly during dry conditions. Transition regions of the dominant backscattering mechanisms at three polarization-combinations, HH-, VV-, and VH-pol, were investigated using σ^0 and VSM at 2 cm because the current models estimate SM within 0–2 cm (Liu, DeRoo, England, & Judge, 2013). The volume scattering model in Eq. (3) was used to demonstrate the plausibility of volume scattering observed from field measurements. Regression analyses, using linear or higher order functions, were conducted to understand the relationship between the σ^0 and VSM for different surface roughness conditions, and R^2 and uncertainties of coefficients obtained using the t-distribution with 95% confidence interval were used to assess the regression.

4.2. Sensitivity analysis

A differential analysis was used to compute the ratio of change in σ^0 to change of the VSM, providing a measure of the sensitivity of σ^0 to VSM, as shown in Eq. (9).

$$\Delta S_{pq} = \frac{\partial \sigma^0_{pq}}{\partial V} \tag{9}$$

where, p and q represent the polarizations of the received and transmitted signal, σ^0 is the backscattering coefficient in dB, and V is the VSM at 2 cm in units of 0.01 m^3/m^3. Student's t-test was conducted to estimate uncertainties in the sensitivity.

Table 3
Measurements of water input during the drydowns.

Drydown	Event description	Water input (mm)	Range of VSM at 2 cm
Period 1	Irrigation on DoY 130.84 for 30 min	3.8	0.03–0.12
Period 2	Irrigation on DoY 139.84 for 15 min	4.4	0.03–0.12
Period 3	Precipitation on DoY 148.95 for 1.5 days	59.6	0.02–0.19
	Precipitation on DoY 151.39 for 45 min	1.6	
	Precipitation on DoY 153.18 for 4 h	5.0	

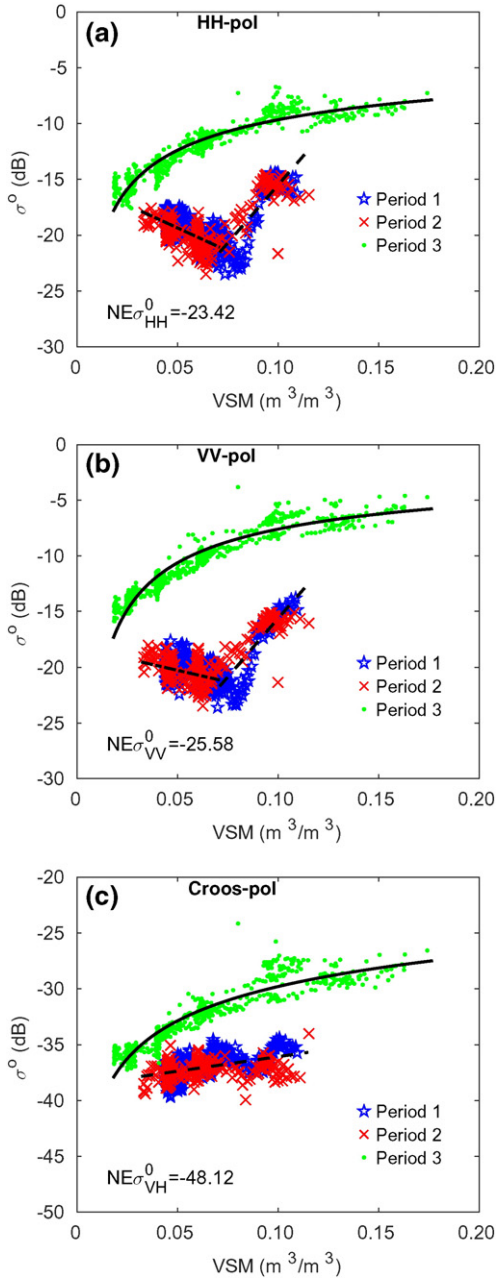

Fig. 4. The scatter plots and regression curves of (a) σ^0_{HH}, (b) σ^0_{VV}, and (c) σ^0_{cr} to VSM observed at 2 cm during period 1 (DoY 130.5–134.5), 2 (DoY 139.7–142.7), and 3 (DoY 148.8–157).

The VSM at 2 cm was chosen for the sensitivity analyses due to the high correlation coefficient, of up to 0.90, between VSM observed at 2 cm to σ^0, consistent with the findings in Liu et al. (2013) and Escorihuela, Chanzy, Wigneron, and Kerr (2010). The theoretical penetration for the L-band could be from 5 cm in wet soils (Zribi, Gorrab, Baghdadi, Lili-Chabaane, & Bernard, 2014) to as deep as 37 cm when VSM is 0.02 m^3/m^3, the lowest SM observed during the experiment. However, even for dry soils a higher correlation of σ^0 to VSM was found at 2 cm than to deeper VSM. In addition, the volume scattering may further decrease the sensitivity of radar backscatter to SM at deeper layers. Observed sensitivities were compared to modeled sensitivity obtained from AIEM. In this study, surface roughness measurements perpendicular to the row were used for AIEM to match the direction of backscatter measurements, where the $\hat{s}$ and $\hat{l}$ were 0.76 and 11.26 cm for smooth soil, and 1.90 and 10.81 cm for rough soil, respectively.

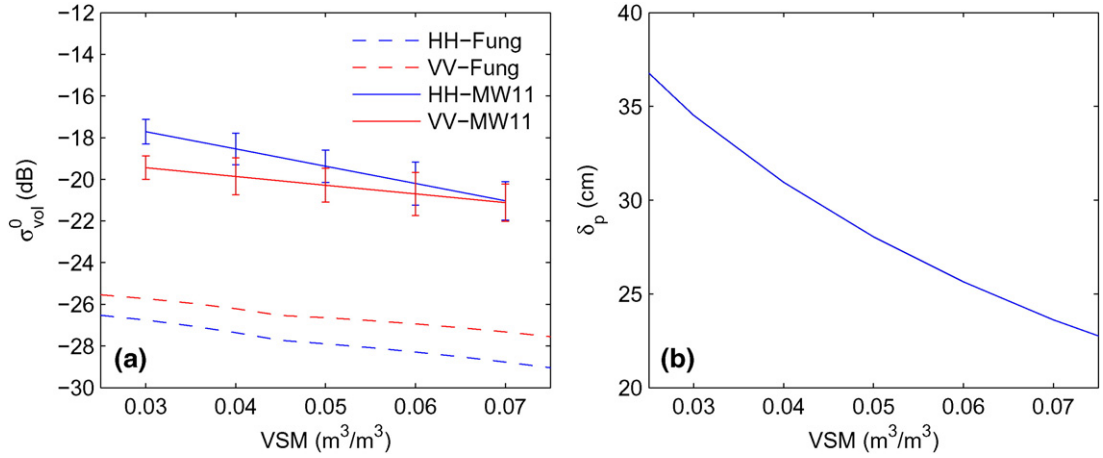

Fig. 5. a) Modeled and observed σ^0_{HH} and σ^0_{VV} with their observation errors when volume scattering dominates the backscattering mechanisms, and (b) the theoretical penetration depth δ_p in terms of VSM.

5. Results and discussion

5.1. Dominant mechanisms of σ^0 in sandy soils during drydown periods

Observed σ^0_{HH}, σ^0_{VV}, and σ^0_{cr} were compared with the observed VSM at 2 cm under different surface roughness conditions, as shown in scatter plots in Fig. 4(a), (b), and (c). Periods 1 and 2, under smooth surface conditions, with *ks* of 0.21 ($k = 2\pi/\lambda$), show that $\sigma^0_{HH}$and σ^0_{VV} increase with decreasing VSM for dry soils, when VSM < 0.07 m^3/m^3. Such a negative-sloped linear relationship between σ^0 and VSM was also found when the zero-order volume scattering was modeled for both VV- and HH-pol at the central frequency of 1.25 GHz and an incidence angle of 40° with the particle size of soil of 3 mm, as shown in Fig. 5(a). When the soil is dry, the radar sees deeper into the soil, up to 37 cm, as shown in Fig. 5(b) using Eq. (4), and thus sees more backscatter from soil particles than under wetter soils. As the soil gets wetter, the extinction coefficient increases and the transmission decreases. Together, these decrease the magnitude of the volume scattering. The transition of the slope of σ^0 with respect to VSM, as shown in Fig. 4(a) and (b), is unprecedented. Such a transition between volume and surface scattering is rarely observed and identified, particularly for sandy soils with a high water drainage rate. The high temporal resolution observations provided added value for monitoring the highly dynamic soil conditions. A pure surface scattering mechanism cannot produce such a negative slope, but we have shown in Fig. 5(a) that a volume scattering mechanism can. This finding is similar to that made in McColl, Entekhabi, and Piles (2014), where the authors attributed the overestimations of SM from the Aquarius scatterometer under smooth, dry soils in a desert to volume scattering. Even though both modeled and observed slopes of σ^0 versus VSM are similar, the modeled σ^0 values are ~7 dB lower than those observed. A scattering model that incorporates higher order scattering between particles and heterogeneity between soil layers may provide a more realistic estimation than the model used in this study. To more fully understand this phenomenon, an intensive field campaign with detailed observations of soil layers and property may also be needed to augment the scattering model.

When the soil got wet and VSM values > 0.07 m^3/m^3, both σ^0_{HH} and σ^0_{VV} increase with VSM, as surface scattering becomes the dominant mechanism. Although return signals at cross-pol under smooth conditions are very low over the smooth periods, the σ^0_{cr} exhibits a very slight positive slope and surface scattering was dominant even during dry conditions. This indicates that the σ^0_{cr} is dominated by surface scattering during dry, smooth soils, and confirms the model simulation using the first order radiative transfer equation (Stogryn, 1974) in that the depolarized backscatter from the soil volume is negligible.

During period 3, the soil was rough as a typical agricultural terrain, with *ks* of 0.5, and σ^0_{HH}, σ^0_{VV}, and σ^0_{cr} consistently increasing with VSM over the range of SM. Unlike the observations during the smooth period, those during the rough period did not exhibit a transition of dominant mechanisms from volume scattering to surface scattering. This indicates that surface scattering was the dominant mechanism under rough conditions during both dry and wet periods. This result is consistent with the findings in Onier et al. (2011) using a comprehensive numerical model to demonstrate that the volume scattering is negligible under rough soils but cannot be ignored under dry, smooth soils. In addition, observed σ^0 at all polarizations for rough soil are significantly higher than those for the smooth soil. This is the regime where surface scattering is dominant and provides a more reliable measurement for SM.

The mechanisms causing the backscatter signal are similar during the two smooth surface drydown periods and were treated together for the analysis. A linear regression using Eq. (10a) was used for all the σ^0 observations during both drydown periods. The co- and cross-pol σ^0 values during the rough period follow a power law with respect to VSM, given as Eq. (10b):

$$\sigma^0_{pq} = a_{pq}V + b_{pq} \tag{10a}$$

$$\sigma^0_{pq} = c_{pq}V^{d_{pq}} \tag{10b}$$

Table 4
Equation coefficients and R^2 of regression results at HH, VV, and cross-pol

	Smooth										Rough				
	0.03 ≤ VSM < 0.07					0.07 ≤ VSM ≤ 0.12					0.02 ≤ VSM ≤ 0.18				
	a	Δ*a*	*b*	Δ*b*	R^2	*a*	Δ*a*	*b*	Δ*b*	R^2	*c*	Δ*c*	*d*	Δ*d*	R^2
HH	−0.83	±0.10	−15.22	±0.47	0.42	2.07	±0.21	−36.25	±1.94	0.69	−22.08	±0.40	−0.36	±0.01	0.88
VV	−0.42	±0.09	−18.18	±0.47	0.16	2.08	±0.18	−36.48	±1.67	0.75	−23.17	±0.55	−0.49	±0.01	0.88
Cr	0.26	±0.04	−38.71	±0.23	0.24	0.26	±0.04	−38.71	±0.23	0.24	−41.28	±0.32	−0.14	±0.01	0.86

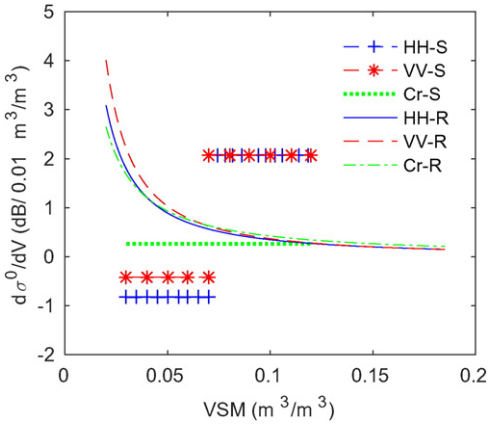

Fig. 6. Sensitivities of observed σ^0_{HH}, σ^0_{VV}, and σ^0_{cr} to VSM at 2 cm VSM during smooth (S) and rough (R) periods.

where σ^0 is in dB, V is the VSM in 0.01 m^3/m^3, a and b are coefficients from the linear regression, and c and d are coefficients from the power law regression.

Overall, measurements of σ^0_{HH}, σ^0_{VV}, and σ^0_{cr} under rough soil conditions closely follow a power law, with R^2 values > 0.86, as shown in Table 4. These results suggest that SM retrieval algorithms utilizing active observations, such as those for the combined active and passive observations using algorithm in (Das et al., 2011), might yield unrealistic SM moisture for dry sandy soils regardless of roughness. When the dry sandy soil is very smooth, surface scattering may no longer be the dominant scattering mechanism. However, even when the dry sandy soil is rough and surface scattering appears dominant, the relationship between σ^0 and SM may not be linear like it was observed at higher SM in previous studies (Dobson & Ulaby, 1986; Kim & van Zyl, 2009; Narayan et al., 2006; Ulaby, Cihlar, & Moore, 1974). Thus, SM retrieval algorithms for sandy soils may need to be adjusted for SM and surface roughness when the SM is <0.10 m^3/m^3.

5.2. Sensitivity of σ^0 to VSM

A differential analysis, as in Eq. (9), is used to obtain the sensitivity of σ^0 to VSM, shown in Fig. 6. Based upon the t-test, uncertainties contained in parameters a, b, c, and d in Table 4 result in an uncertainty of <0.21 dB/0.01m^3/m^3 for smooth soils, and <0.18 dB/0.01m^3/m^3 for rough soils. When surface scattering is dominant, σ^0_{VV} and σ^0_{HH} exhibit similar sensitivities to SM for smooth soil, but σ^0_{VV} is more sensitive to SM than σ^0_{HH} by up to 1 dB/0.01m^3/m^3 for rough soil. When the soil becomes wetter, these differences decrease to <0.1 dB/0.01m^3/m^3 and sensitivities at both polarizations are lower. For the rough soils, the sensitivity is stronger in the dry than wet conditions because the observed σ^0 to VSM follows a power law relationship, indicating the stronger change in the dry end of the soil. Such a relationship can also be described theoretically using physical optics (PO), where the co-pol backscatter is a function of Fresnel reflection coefficient, the zeroth order term in PO, following a power law with respect to VSM (De Roo, 1996).

The sensitivity values are significantly higher, by as much as 1.8 dB/0.01m^3/m^3, for smooth surfaces than for rough surfaces, because surface roughness tends to mask the sensitivity to SM (Lakshmi, 2013). Although higher sensitivity is observed for the smooth soil, the low returns from smooth soils may permit mechanisms other than surface scattering, such as volume scattering, to become important during dry conditions. Ambiguity arises because the σ^0-VSM curve is not monotonic when the soil is sufficiently smooth, and volume scattering dominates surface scattering for low VSM values. This can complicate a VSM estimation using a surface scattering model, as is typically done in current algorithms. For rough surfaces, active microwave observations are dominated by surface scattering, and are more amenable to SM estimation. Modeled and observed sensitivities were compared to understand the potential impacts of VSM and roughness conditions on estimates of σ^0 from the AIEM. Fig. 7(a) and (b) show the σ^0_{HH} and σ^0_{VV} estimated by AIEM as functions of VSM. Overall, the absolute differences between the observed and modeled σ^0 at both polarizations are as high as 4 dB and 6 dB under rough and smooth soils, respectively. The inconsistency between the model simulation and observations could be from the gradient of the soil moisture in the top surface, errors in the surface roughness measurements and the correction equations (Eqs. (1a) and (1b)), and the model itself (Liu et al., 2013; Rondinelli et al., 2015). However, this study was to provide plausible scenarios to explain the behaviors of scattering mechanisms and did not intend to match the model simulation and observations for SM retrieval. The σ^0 at both polarizations follow a power law, similar to the observed relationship for rough soil, but different from that of smooth soil. Because AIEM is a surface backscattering model, it does not capture the volume scattering observed from the smooth, dry soils. Sensitivity of σ^0_{VV} is slightly higher than that of σ^0_{HH} by about 0.18 dB/0.01m^3/m^3, (see Fig. 8). Surface roughness does not significantly affect sensitivities of modeled σ^0 to VSM, as the difference between smooth and rough soil conditions is < 0.08 dB/0.01m^3/m^3. Although the modeled sensitivity using AIEM is nearly independent of surface roughness, observations in the previous studies and this study have shown the sensitivity of σ^0 to VSM varies under different roughness conditions (Aubert et al., 2011; Narvekar, Entekhabi, Kim, & Njoku, 2015; Ulaby, Batlivala, & Dobson, 1978; Wang, Engman, Mo, Schmugge, & Shiue, 1987). When surface scattering is the dominant mechanism, the AIEM underestimates

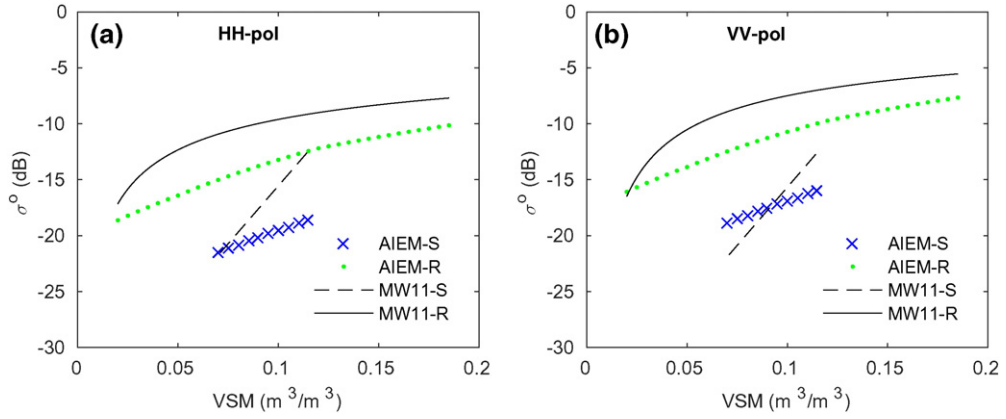

Fig. 7. The regression curves of observed and modeled (a) σ^0_{HH} and (b) σ^0_{VV} vs VSM observed at 2 cm during smooth and rough periods, when surface scattering dominates. In the legend, S and R indicate smooth and rough soils, respectively.

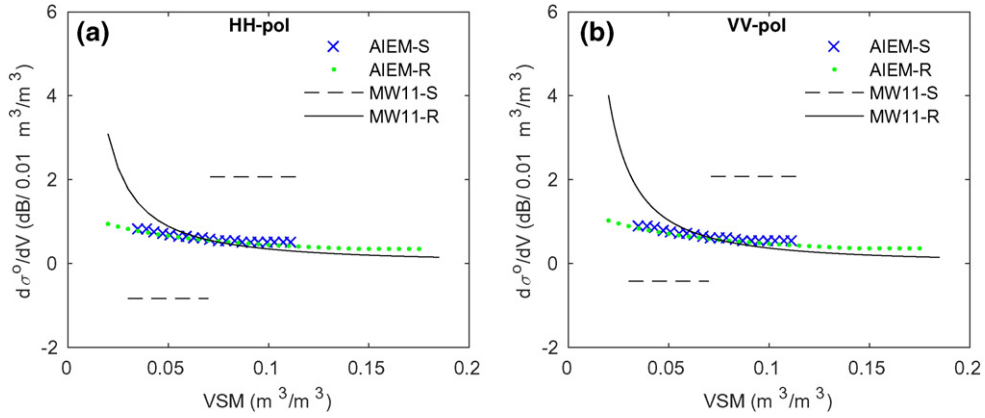

Fig. 8. The sensitivity of modeled and observed (a) σ^0_{HH} and (b) σ^0_{VV} to VSM at 2 cm during smooth and rough periods. In the legend, S and R indicate smooth and rough soils, respectively.

sensitivities by as much as 1.8 during smooth soils, and by as much 3 dB/0.01m^3/m^3 when SM < 0.05 m^3/m^3 during rough soils.

6. Summary and conclusions

This study investigates the dominant mechanisms of backscattering from bare sandy soils, using high temporal density of observations, under different moisture for smooth and rough surfaces conditions. Evidence of a dominant scattering mechanism other than surface scattering, such as volume scattering, was demonstrated at both HH and VV polarizations, under dry, smooth soil condition when VSM < 0.07 m^3/m^3, with *ks* of 0.21. Observations at HH-, VV-, and cross-pol for rough surface follow a power law with R^2 values of 0.88, 0.88, and 0.86, suggesting that retrieval algorithms developed based upon a linear relation between σ^0 and VSM may be less than optimal for SM retrieval. Although observed σ^0 at co-pol for smooth soil show higher sensitivity to VSM than those under rough soil by up to 1.8 dB/0.01m^3/m^3, a certain level of roughness might be important for a dry soil to obtain adequate surface scattering and to avoid retrieval during times when volume scattering is the dominant mechanism. When surface scattering is the dominant mechanism, the AIEM underestimates sensitivity for both smooth and rough soils, indicating that the real surface might contain different backscattering mechanisms. These findings offer insights into retrieval and assimilation algorithms using active signatures for sandy, agricultural fields. Further studies of bare soil backscatter mechanisms under extreme and dynamic conditions for other soil types are suggested.

Acknowledgment

This research and MicroWEX was supported by the NASA-Terrestrial Hydrology Program-NNX09AK29G.

References

Aubert, M., Baghdadi, N., Zribi, M., Douaoui, A., Loumagne, C., Baup, F., ... Garrigues, S. (2011). Analysis of TerraSAR-X data sensitivity to bare soil moisture, roughness, composition and soil crust. *Remote Sensing of Environment, 115*, 1801–1810.

Baghdadi, N., Paillou, P., Grandjean, G., & Davidson, M. (2000). Relationship between profile length and roughness parameters for natural surfaces. *International Journal of Remote Sensing*, 3375–3381.

Balenzano, A., Satalino, G., Lovergine, F., Rinaldi, M., Iacobellis, V., Mastronardi, N., & Mattia, F. (2013). On the use of temporal series of L- and X-band SAR data for soil moisture retrieval. Capitanata plain case study. *European Journal of Remote Sensing, 46*, 721–737.

Barrett, B., Dwyer, E., & Whelan, P. (2009). Soil moisture retrieval from active spaceborne microwave observations: An evaluation of current techniques. *Remote Sensing, 1*, 210–242.

Bongiovanni, T., Liu, P. W., Nagarajan, K., Preston, D., Rush, P., Duan, X., ... England, A. (2015). Field observations during the Tenth Microwave, Water, and Energy Balance Experiment (MicroWEX-10): from March 1, 2011 through January 5, 2012. *Technical Report*. Center for Remote Sensing, University of Florida (http://edis.ifas.ufl.edu/pdffiles/AE/AE512.pdf).

Chen, K., Wu, T., Tsang, L., Li, Q., Shi, J., & Fung, A. (2003). Emission of rough surfaces calculated by the integral equation method with comparison to three-dimensional moment method simulations. *IEEE Transactions on Geoscience and Remote Sensing, 41*, 90–101.

Das, N., Entekhabi, D., & Njoku, E. (2011). An algorithm for merging SMAP radiometer and radar data for high-resolution soil-moisture retrieval. *IEEE Transactions on Geoscience and Remote Sensing, 49*, 1504–1512.

De Roo, R. (1996). *Theory and measurement of bistatic scattering of X-band microwaves from rough dielectric surfaces.* Ph.D. thesis Ann Arbor, Michigan, USA: Univ. of Michigan.

Dobson, M., & Ulaby, F. (1986). Active microwave soil moisture research. *IEEE Transactions on Geoscience and Remote Sensing, GE-24*, 23–36.

Escorihuela, M., Chanzy, A., Wigneron, J. P., & Kerr, Y. (2010). Effective soil moisture sampling depth of L-band radiometry: A case study. *Remote Sensing of Environment, 114*, 995–1001.

Fung, A. (1994). *Microwave scattering and emission models and their applications.* Norwood, MA: Artech House.

Fung, A., & Kuo, N. (2006). Backscattering from multi-scale and exponentially correlated surfaces. *Journal of Electromagnetic Waves and Applications, 20*, 3–11.

Hoekman, D. (1991). Speckle ensemble statistics of logarithmically scaled data. *IEEE Transactions on Geoscience and Remote Sensing, 29*, 180–182.

Judge, J. (2007). Microwave remote sensing of soil water: Recent advances and issues. *Transactions of the ASABE, 50*, 1645–1649.

Kim, Y., & van Zyl, J. (2009). A time-series approach to estimate soil moisture using polarimetric radar data. *IEEE Transactions on Geoscience and Remote Sensing, 47*, 2519–2527.

Kim, Y., Jackson, T., Bindlish, R., Lee, H., & Hong, S. (2012). Radar vegetation index for estimating the vegetation water content of rice and soybean. *IEEE Geoscience and Remote Sensing Letters, 9*, 564–568.

Kurum, M., O'Neill, P., Lang, R., Cosh, M., Joseph, A., & Jackson, T. (2011). Impact of conifer forest litter on microwave emission at L-band. *IEEE Transactions on Geoscience and Remote Sensing, 50*, 1071–1084.

Lakshmi, V. (2013). Remote sensing of soil moisture. *ISRN Soil Science, 2013*. http://dx.doi.org/10.1155/2013/424178.

Liu, P. W., DeRoo, R., England, A., & Judge, J. (2013). Impact of moisture distribution within the sensing depth on L- and C-band emission in sandy soils. *IEEE Journal of Selected Topics in Applied Earth Observations and Remote Sensing (JSTARS), 6*, 887–899.

McColl, K., Entekhabi, D., & Piles, M. (2014). Uncertainty analysis of soil moisture and vegetation indices using Aquarius scatterometer observations. *IEEE Transactions on Geoscience and Remote Sensing, 52*, 4259–4272.

Mironov, V., & Bobrov, P. (2009). *Spectroscopic microwave dielectric model of moist soils.* INTECH Open Access Publisher.

Mironov, V., Kosolapova, L., & Fomin, S. (2009). Physically and mineralogically based spectroscopic dielectric model for moist soils. *IEEE Transactions on Geoscience and Remote Sensing, 47*, 2059–2070.

Nagarajan, K., Liu, P. W., DeRoo, R., Judge, J., Akbar, R., Rush, P., ... Terwilleger, R. (2014). Automated L-band radar system for sensing soil moisture at high temporal resolution. *IEEE Geoscience and Remote Sensing Letters, 11*, 504–508.

Narayan, U., Lakshmi, V., & Jackson, T. (2006). High-resolution change estimation of soil moisture using L-band radiometer and radar observations made during the SMEX02 experiments. *IEEE Transactions on Geoscience and Remote Sensing, 44*, 1545–1554.

Narvekar, P., Entekhabi, D., Kim, S., & Njoku, E. (2015). Soil moisture retrieval using L-band radar observations. *IEEE Transactions on Geoscience and Remote Sensing, 53*, 3492–3506.

Nashashibi, A., Ulaby, F., & Sarabandi, K. (1996). Measurement and modeling of the millimeter-wave backscatter response of soil surfaces. *IEEE Transactions on Geoscience and Remote Sensing, 34*, 561–572.

Nishimoto, M. (2010). Characteristics of rough surface parameters estimated from measured surface profile of finite length. *IEEE Int. Geosc. and Rem. Sens. Symposium, Proc. IGARSS 2010* (pp. 4436–4439).

Oh, Y., Sarabandi, K., & Ulaby, F. (1992). An empirical model and an inversion technique for radar scattering from bare soil surfaces. *IEEE Transactions on Geoscience and Remote Sensing, 30*, 370–381.

Oh, Y., Sarabandi, K., & Ulaby, F. (2002). Semi-empirical model of the ensemble-averaged differential Mueller matrix for microwave backscattering from bare soil surfaces. *IEEE Transactions on Geoscience and Remote Sensing, 40*, 1348–1355.

Onier, C., Chanzy, A., Chambarel, A., Rouveure, R., Chanet, M., & Bolvin, H. (2011). Impact of soil structure on microwave volume scattering evaluated by a two-dimensional numerical model. *IEEE Transactions on Geoscience and Remote Sensing, 49*, 415–425.

Paillou, P., Grandjean, G., Baghdadi, N., Heggy, E., August-Bernex, T., & Achache, J. (2003). Subsurface imaging in south-central Egypt using low-frequency radar: Bir Safsaf revisited. *IEEE Transactions on Geoscience and Remote Sensing, 41*, 1672–1684.

Rondinelli, W., Hornbuckle, B., Patton, J., Cosh, M., Walker, V., Carr, B., & Logsdon, S. (2015). Different rates of soil drying after rainfall are observed by the SMOS satellite and the South Fork in situ soil moisture network. *Journal of Hydrometeorology, 16*, 889–903.

Rosen, P., Hensley, S., Shaffer, S., Veilleux, L., Chakraborty, M., Misra, T., ... Satish, R. (2015). The nasa-isro sar mission - an international space partnership for science and societal benefit. *Radar Conference (RadarCon), 2015 IEEE* (pp. 1610–1613). http://dx.doi.org/10.1109/RADAR.2015.7131255.

Schaber, G., McCauley, J., Breed, C., & Olhoeft, G. (1986). Shuttle image radar: physical controls on signal penetration and subsurface scattering in the eastern Sahara. *IEEE Transactions on Geoscience and Remote Sensing, GE-24*, 603–623.

Shi, J., van Zyl, J., Soares, J., & Engman, E. (1992). Retrieval bare-soil moisture using L-band SAR. *International Archives of Photogrammetry and Remote Sensing, 29*(Part B7), 595–597.

Stogryn, A. (1974). Electromagnetic scattering by random dielectric constant fluctuations in a bounded medium. *Radio Science, 9*, 509–518.

Suzuki, S., Osawa, Y., Hatooka, Y., Kankaku, Y., & Watanabe, T. (2009). Soverview of Japan's advanced land observing satellite-2 mission. *Proceedings of SPIE, 7474*. http://dx.doi.org/10.1117/12.831340.

Ulaby, F., & Dobson, M. (1989). *Handbook of radar scattering statistics for terrain*. Norwood, MA: Artech House.

Ulaby, F., Batlivala, P., & Dobson, M. (1978). Microwave backscatter dependence on surface roughness, soil moisture, and soil texture: Part 1—Bare soil. *IEEE Transactions on Geoscience and Remote Sensing, GE-16*, 286–295.

Ulaby, F., Cihlar, J., & Moore, R. (1974). Active microwave measurement of soil water content. *Remote Sensing of Environment, 3*, 185–203.

Ulaby, F., Kouyate, F., Fung, A., & Sieber, A. (1982a). A backscattering model for a randomly perturbed periodic surface. *IEEE Transactions on Geoscience and Remote Sensing, GE-20*, 518–528.

Ulaby, F., Moore, R., & Fung, A. (1981). *Microwave remote sensing: Active and passive, Vol. I*, Boston, MA: Artech House.

Ulaby, F., Moore, R., & Fung, A. (1982b). *Microwave remote sensing: Active and passive, Vol. II*, Boston, MA: Artech House.

Ulaby, F., Moore, R., & Fung, A. (1986). *Microwave remote sensing: Active and passive, Vol. III*, Boston, MA: Artech House.

USDA (1987). Soil mechanics level I: Module 3-USDA textural soil classification study guide. *Technical Report*. Soil Conservation Service, United States Department of Agriculture (http://www.wcc.nrcs.usda.gov/ftpref/wntsc/H&H/training/soilsOther/soil-USDA-textural-class.pdf).

Wang, J., Engman, E., Mo, T., Schmugge, T., & Shiue, J. (1987). The effects of soil moisture, surface roughness, and vegetation on L-Band emission and backscatter. *IEEE Transactions on Geoscience and Remote Sensing, GE-25*, 825–833.

Wu, T., Chen, K., Shi, J., Lee, H., & Fung, A. (2008). A study of an AIEM model for bistatic scattering from randomly rough surfaces. *IEEE Transactions on Geoscience and Remote Sensing, 46*, 2584–2598.

Yang, M., Tien, K., Casanova, J., & Judge, J. (2005). Measurements of soil surface roughness during the Fourth Microwave Water and Energy Balance Experiment: April 18 through June 13, 2005. *Technical Report*. Center for Remote Sensing, University of Florida (http://edis.ifas.ufl.edu/AE363).

Zribi, M., Gorrab, A., Baghdadi, N., Lili-Chabaane, Z., & Bernard, B. (2014). Influence of radar frequency on the relationship between bare surface soil moisture vertical profile and radar backscatter. *IEEE Geoscience and Remote Sensing Letters, 11*, 848–852.